

Testing gravitational redshift based on microwave frequency links onboard China Space Station

Wenbin Shen,^{1,2,3,*} Pengfei Zhang,^{1,2} Ziyu Shen,^{4,†} Rui Xu,^{1,2} Xiao Sun,³ Mostafa Ashry,^{1,2,3} Abdelrahim Ruby,^{1,2,3} Wei Xu,^{1,2} Kuangchao Wu,^{1,2} Yifan Wu,^{1,2} An Ning,^{1,2} Lei Wang,^{1,2} Lihong Li,^{1,2} and Chenghui Cai^{1,2}

¹*School of Geodesy and Geomatics, Wuhan University, Wuhan 430079, China.*

²*Time and Frequency Geodesy Center, Wuhan University, Wuhan 430079, China.*

³*State Key Laboratory of Information Engineering in Surveying, Mapping and Remote Sensing, Wuhan University, Wuhan 430079, China.*

⁴*School of Resource, Environmental Science and Engineering, Hubei University of Science and Technology, Xianning, Hubei, China.*

(Dated: April 27, 2022)

In 2022 China Space Station (CSS) will be equipped with atomic clocks and optical clocks with stabilities of 2×10^{-16} and 8×10^{-18} , respectively, which provides an excellent opportunity to test gravitational redshift (GRS) with higher accuracy than previous results. Based on high-precise frequency links between CSS and a ground station, we formulated a model and provided simulation experiments to test GRS. Simulation results suggest that this method could test the GR at the accuracy level of $(0.27 \pm 2.15) \times 10^{-7}$, more than two orders in magnitude higher than the result of the experiment of a hydrogen clock on board a flying rocket more than 40 years ago.

I. INTRODUCTION

Scientists paid great attention to testing the gravitational redshift (GRS) effect, one of three classic predictions of general relativity theory (GRT). In 1976 scientists conducted the Gravity Probe-A (GP-A) experiment mission to test GRS [1]. A hydrogen atomic clock was on board a rocket in this mission, which flew about two hours in space. Based on the microwave links between the rocket and several ground stations, the GP-A experiment has tested the GRS at the accuracy level of 7×10^{-5} . To improve the accuracy level, one should consider two aspects. In one aspect, we try to use better clocks with higher stability and accuracy. In another aspect, we try to create a condition that the gravitational potential difference between two points is as significant as possible. For instance, using optic clocks with stabilities around 10^{-18} , Katori's group [2] measured a height of 450 m with an accuracy of 4.1 cm, by which the accuracy of testing GRS achieves 9.1×10^{-5} , a little worse than the previous rocket-experiment result of 7×10^{-5} [3]. Another example, based on observations from two eccentric-orbit Galileo satellites E14 and E18 (the stabilities of the onboard clocks are around 10^{-15} /day), several groups tested GRS with an accuracy level around $2.5 \sim 4.5 \times 10^{-5}$ [4–6].

Recently, a few space atomic clock projects have been put forward. For example, the Atomic Clock Ensemble in Space (ACES) mission onboard the international space station (ISS) and the China Space Station (CSS) mission. The ACES mission will be equipped with an atomic clock with long-term stability 2×10^{-16} [7, 8], and use its two independent time and frequency transfer

links, including three microwave links (MWL) and two European Laser Timing (ELT) optical links to distribute time and frequency scale to the ground stations. By using one uplink and two downlinks MWL, a tri-frequency combination method for time-frequency transfer is constructed according to the accuracy of the ACES atomic clock [9, 10]. Verified by simulation experiments the tri-frequency combination method may test GRS at a level of 10^{-6} [11, 12]. The CSS and ACES are different in design. The CSS will be equipped with an optical atomic clock whose long-term stability is 8×10^{-18} [11–14], and two up-microwave links from a ground station to CSS and two down-microwave links from CSS to the ground station will be established. One uplink signal and one downlink signal have the same frequency of 30.4 GHz but different circular polarization directions. Considering the MWL characters, the errors caused by the propagation will be eliminated. This study created a new frequency transfer model used in the space-ground frequency transfer to test GRS, which is at least an order of magnitude higher than the results given by previous studies.

II. CHINA SPACE STATION

The CSS designed three modules, one core module (CM) and two experiment modules (EM). The CSS has recently been launched to an orbit with a height around 400 km above the ground since April 29, 2021. From June 17 to September 16, 2021, three Chinese astronauts stayed in the TianHe core module of CSS to prepare for future experiments. Since October 16, another three Chinese astronauts have been successively launched in the core module for further preparatory work. The CSS will stay in orbits for at least ten years. For the purpose of time and frequency applications, three or more ground stations have been or will be established, including for

* 2891983829@qq.com

† theorhythm@foxmail.com

instance Beijing, Xi'An, Shanghai, and Wuhan stations. In addition, it will be established the space-ground signals links between CSS and ground stations, including microwave links and laser links.

Experiments module II will be equipped with a set of clocks attached to the core module moving in orbit in September 2022. The set of clocks consists of a hydrogen clock with daily stability of 2×10^{-15} , a cold-atom microwave fountain clock with daily stability of 2×10^{-16} , and an optical atomic clock with long-term stability of 8×10^{-18} [11–14]. There will be four microwave links between CSS and a ground station of interest for time and frequency transfer. The MWL consist of two up-links and two downlinks as listed in Table I. Compared with the ACES mission, there are two changes. One is that the CSS mission has an additional uplink with its frequency equal to the frequency of one of the downlink signal. Another is that the uplink and downlink signals are left-hand and right-hand circularly polarized, respectively. In ACES, there are three microwave signals without polarization, hence it is designed that the three signals have different frequencies to distinguish the up and downlinks. While, for the CSS mission when a microwave signal is polarized, incident upon an antenna from a given direction, it will be received by the antenna with same polarization character (say both right-hand circularly polarized). This technology is referred to as polarization match. The antenna with corresponding polarization character is selected according to different polarization natures of the microwaves to distinguish the uplink and downlink signals [15].

Here we use only the uplink and downlink signals both with frequency 30.4 GHz (see Fig. 1), and other two links with different frequencies (see Table I) will not be used in this study. Since the frequencies of the uplink and downlink are the same, the uninterested frequency shifts caused by the Doppler effects, troposphere and ionosphere effects are the same. Making a difference between the up and downlinks, we may cancel the uninterested frequency shifts and double the GRS, which provides an opportunity to test GR with higher accuracy.

III. RELATIVISTIC MODEL FOR FREQUENCY TRANSFER OF THE CSS

The up-link and down-link signals between CSS (denoted as S) and ground station (denoted as E) satisfy the following expression:

$$\begin{aligned} f_{I,J}^r &= f_{I,J}^e - \Delta U_{IJ} + \Delta f_{\text{Dop1}-IJ} + \Delta f_{\text{Dop2}-IJ} \\ &+ \Delta f_{\text{tro}-IJ} + (\Delta f_{\text{ion1}-IJ} + \Delta f_{\text{ion2}-IJ}) \\ &- \Delta f_{\text{ti}-IJ} - \Delta f_{\text{pl}-IJ} + \varepsilon_{IJ} \end{aligned} \quad (1)$$

where $I, J = E, S, I \neq J$, E and S denote Earth and space station, respectively; $f_{I,J}^r$ is the received frequency of the signal at J coming from I , $f_{I,J}^e$ is the emitting frequency of the signal at I toward J ; $\Delta U_{IJ} = U_J - U_I$,

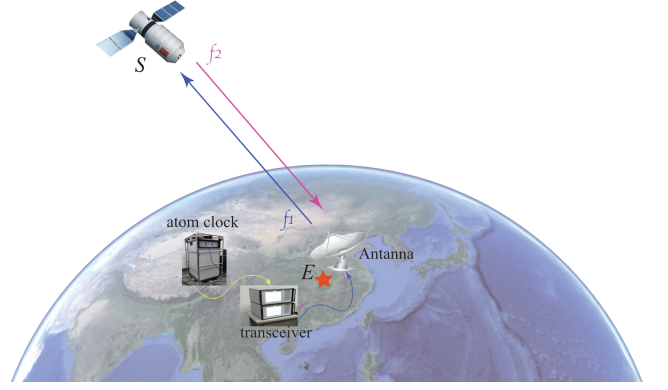


FIG. 1. One up-link and one down-link of microwave signals between the China Space Station (CSS) noted as S and a ground station (E) at Wuhan, China. The up-link (f_1) and down-link (f_2) are respectively left- and right-hand circularly polarized signals both with the frequency 30.4 GHz. The antenna and the atomic clock at ground are linked by a transceiver. The received signals from CSS are compared with the local signals generated by the ground clock.

U_I is the gravitational potential at I , $\Delta f_{\text{Dop1}-IJ}$ and $\Delta f_{\text{Dop2}-IJ}$ are the first and second order Doppler frequency shifts of the signals transmitting from I to J , $\Delta f_{\text{tro}-IJ}$ is the frequency shift of the signal transmitting from I to J caused by the troposphere, $\Delta f_{\text{ion1}-IJ}$ and $\Delta f_{\text{ion2}-IJ}$ are the first- and second-order frequency shifts of the signal transmitting from I to J caused by the ionosphere, $\Delta f_{\text{ti}-IJ}$ and $\Delta f_{\text{pl}-IJ}$ are frequency shifts caused by tides and external celestial bodies (including the sun, moon, Mercury, Venus, Mars, Jupiter, etc.), respectively, ε_{IJ} are the un-modeled errors of the signals transmitting from I to J , including for instance the clock errors, random errors and other noises. As presently designed in CSS, the uplink signal with frequency $f_1 = 30.4$ GHz is left-hand circularly polarized, and the downlink signal with frequency $f_2 = 30.4$ GHz is right-hand circularly polarized [13, 14]. Hence, we have $\Delta f_{\text{ion2}-ES} = \Delta f_{\text{ion2}-SE}$ [16]. In addition, taking into account the following relationships, $\Delta U_{IJ} = -\Delta U_{JI}$, $\Delta f_{\text{Dop1}-IJ} = \Delta f_{\text{Dop1}-JI}$, $\Delta f_{\text{Dop2}-IJ} = \Delta f_{\text{Dop2}-JI}$, $\Delta f_{\text{tro}-IJ} = \Delta f_{\text{tro}-JI}$, $\Delta f_{\text{ion1}-IJ} = \Delta f_{\text{ion1}-JI}$, $\Delta f_{\text{ti}-IJ} = -\Delta f_{\text{ti}-JI}$, and $\Delta f_{\text{pl}-IJ} = -\Delta f_{\text{pl}-JI}$, from Eq. (1), subtracting f_{ES}^r from f_{SE}^r , we obtain

$$\Delta U_{SE} = \frac{f_{SE}^r - f_{ES}^r}{2} - \Delta f_{\text{ti}-SE} - \Delta f_{\text{pl}-SE} + \varepsilon \quad (2)$$

where $\varepsilon = -(\varepsilon_{SE} - \varepsilon_{ES})/2$. On the right-hand side of Eq. (2), the first term is directly observed. The second and third terms, $\Delta f_{\text{ti}-SE}$ and $\Delta f_{\text{pl}-SE}$, can be calculated by relevant models. For instance, the tides can be corrected by the software ETERNA [17–19], and general formulas can directly correct the influences by external celestial bodies [20, 21]. In Eq. (2), both the first- and second-order ionospheric frequency shifts vanish because one left-hand (up-link) and another right-hand (down-link) circularly polarized wave signals are designed in

TABLE I. Parameters of China Space Station (CSS) and frequency links.

| Parameter | Value |
|------------------------------------|-----------------------------------------------------------|
| Altitude | ~400 km |
| Uplink frequency | 30.4 GHz, 26.8 GHz (both left-hand circularly polarized) |
| Downlink frequency | 30.4 GHz, 20.8 GHz (both right-hand circularly polarized) |
| Orbit inclination | 41.5° |
| Minimum visible elevation angle | 5° |
| Observation cutoff elevation angle | 15° |

CSS. In practice, since Eq.(2) is not rigorous, and the uplink signal's path does not coincide with the downlink signal's path, after the combination of the up and down frequency signals, there are still following residual errors: first- and second-order Doppler frequency shifts, troposphere frequency shift, ionosphere frequency shift, as shown in Table II.

At a given time t , we can obtain an observation of ΔU_{ES} . Comparing the observation with the corresponding true (model) value ΔV_{ES} , we can get the offset between the observed value and the model value, expressed in relative difference as

$$\alpha = \frac{\Delta U(t)_{ES} - \Delta V(t)_{ES}}{V(t)_{ES}} \quad (3)$$

which describes the deviation of the observed result based on GRT from the true (model) value. If GRT holds, $\alpha = 0$.

IV. SIMULATION EXPERIMENTS

In our simulation experiments, we chose Luojia time and frequency station (LTFS) at Wuhan as the ground station, the coordinate of which is (30°31'51.90274" N, 114°21'25.83516" E, 25.728 m). The CSS parameters and signals' original emitted frequency values are shown in Table I. The observations in our simulation experiments are the received frequency signals between the ground station LTFS and CSS, denoted as f_{IJ}^r , which includes various frequency shifts caused by different factors, as expressed by Eq. (1). Here we simulate the first-order Doppler frequency shifts, relativistic frequency shifts (including gravitational redshift and second-order Doppler effect), atmospheric frequency shift, tidal frequency shift, and clock noises to obtain the received frequency values.

In the simulation experiments, we set the stability of the onboard optical clock of CSS as $2 \times 10^{-15}/s$, and its long-term stability is about 8×10^{-18} . The other effects that appeared in Eq. (1) are simulated by the orbit parameters data, which can be downloaded from <http://www.celestrak.com/NORAD/elements/stations.txt>, including the position, velocity, and acceleration information about the CSS. To obtain a better result, we set the observation cutoff elevation angle of the CSS larger than 15°. In the simulation, the accuracies of radial

orbit position and velocity are set as 10 cm and 1 mm/s, respectively [11, 12].

In the simulation of the atmospheric effects on the frequency, we select the Saastamoinen model [22], VMF1(Vienna Mapping Function) [23], and meteorological parameters in the space region near and around the LTFS to simulate the tropospheric frequency shifts. We select IRI (International Reference Ionosphere) model [24] and IGRF-13 (international geomagnetic reference field) model [25] to simulate the first- and second-order ionospheric frequency shifts. We use the IERS (International Earth Rotation and Reference Systems) Convention 2010 [26] to calculate the tidal harmonic parameters and consequently simulate the frequency shifts caused by the tidal effect.

According to the simulation setup, we may obtain the observed values f_{IJ}^r based on emitting frequency values. By Eq. (2), the value of ΔU_{SE} could be calculated. We use EGM2008 model [27] to calculate the gravitational potentials at CSS and ground station to obtain ΔV_{ES} as the true value.

We have conducted simulation experiments to estimate the feasibility of a GRS test based on CSS. The experiment lasts for one day, from May 22 00:00 to May 23 00:00, 2021. The orbit data were generated by a Two-line Element Set (TLE) [28], which is used to describe a spacecraft orbit and to predict its position and velocity. The trace of CSS during one day was depicted in Fig. 2. The gravitational potential at the space station was calculated by EGM2008 [29]. The precision of EGM2008 is about several centimeters at the CSS' orbit. The ground station LTFS is located at Wuhan, China, and its gravitational potential can be determined by leveling at the precision of centimeter-level or better. Suppose $\alpha = 0$, and then we can calculate the true GRS value (model value) based on the general relativity theory (GRT).

The next step is considering various error sources and simulating the observation values for a real case. For example, one of the primary error sources in the GRS test is clock instability. In our experiment the stability of on-board clock is set as $2 \times 10^{-15}/\sqrt{\tau}$ (τ in second), same stability as the designed by CSS mission. The stability of ground clock is supposed to be better, reaching $1 \times 10^{-15}/\sqrt{\tau}$.

According to Allan [30], the clock noises are classified as five different types of stochastic noises, including

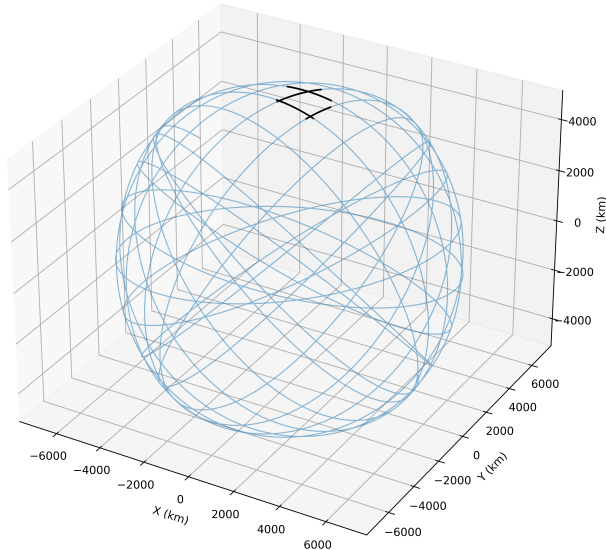


FIG. 2. The orbit of CSS in Earth Centered Earth Fix (ECEF) coordinates during the observations in one day. The ground station is located at Wuhan, China ($30^{\circ}31'51.90274''$ N, $114^{\circ}21'25.83516''$ E, 25.728 m). The observation period is from June 1, 00:00 to June 2, 00:00, 2021. The light-colored dash lines denote when the CSS and CSS and Wuhan station are not intervisible. The solid black lines denote when CSS and Wuhan station are intervisible and observation values are available.

Random Walk Frequency Modulation (RWFM), Flicker Frequency Modulation (FFM), White Frequency Modulation (WFM), Flicker Phase Modulation (FPM) and White Phase Modulation (WPM). We analyzed the ratios of the five kinds of noises to the clock signals and restore the clock signals according to the different ratios. We set the stabilities of ground clock and on-board clock as $1.0 \times 10^{-15}/\sqrt{\tau}$ and $2.0 \times 10^{-15}/\sqrt{\tau}$, respectively (see Table II). Then we use a python library Allantools (<https://github.com/aewallin/allantools>) to generate the series of clock frequency errors based on the characteristics of atomic clocks. Their total Allan deviations [30] are depicted in Fig. 3. Another important influence factor is the frequency shift caused by the atmosphere. The local weather station can record the meteorological elements of the ground station. Then, the signal's tropospheric frequency shift can be estimated based on the GPT2-mapping function. The ionospheric frequency shift can be calculated according to International Reference Ionosphere (IRI) model [31]. The precision of the atmosphere model is regarded as residual errors and added to the frequency shift observation. Other error sources such as the orbit error of CSS, the EGM2008 error, tidal correction residual are also considered. Each of them is simulated as Gaussian errors plus a randomly set systematic offset. The magnitudes of error sources are listed in Table II.

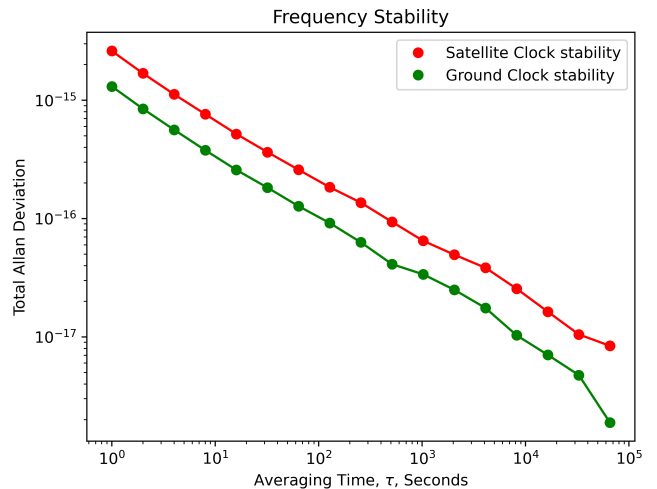


FIG. 3. The total Allan deviation of the clocks' frequency stability. The stability of on-board clock is about $2.0 \times 10^{-15}/\sqrt{\tau}$ (τ in second), and the stability of ground clock is about $1.0 \times 10^{-15}/\sqrt{\tau}$.

Once the simulated observation frequency values are obtained, they are compared with the true frequency shift values and part of the offset between them (a short period lasts for about 5 minutes) are depicted in Fig. 4. We can see that the most prominent offset component comes from clock error, which is at least two magnitudes larger than other error influences. The influence of ionosphere frequency shift shows apparent fluctuation because the total electron content (TEC) distribution varies at different latitudes, and the extent of path discrepancy of uplink and downlink signal also varies at different elevating angles.

There are four sections (periods) in which observation data are available (see the solid black line in Fig. 2) during the one day's experiment. The result of one-day experiment is $0.17 \pm 3.05 \times 10^{-16}$, where 0.17×10^{-16} is the mean offset between the true value and the experiment result, corresponding to 1.68×10^{-7} for the offset of α , and $\pm 3.05 \times 10^{-16}$ is the uncertainty (STD). The offset of α reflects the precision of the GRS test experiment. However, the result of only one simulation experiment might be influenced by accidental factors. Therefore, we repeated the above experiment 40 times for the same day under different random seeds of errors generation to estimate the precision of the GRS test, and the results of α offset of 40 experiments are depicted in Fig. 5. We can see that the mean offset of α is 2.7×10^{-8} , with the standard deviation of 2.15×10^{-7} .

V. CONCLUSION

Based on the uplink and downlink frequency signals in free space between the CSS and a ground station, we established a formulation for determining the grav-

TABLE II. Error sources and their magnitudes in the simulation experiments.

| Error sources | Magnitudes |
|----------------------------------------|-----------------------------------------------------------------------------------|
| On-board clock stability | $2.0 \times 10^{-15} / \sqrt{\tau}$ |
| Ground clock stability | $1.0 \times 10^{-15} / \sqrt{\tau}$ |
| Troposphere influence residual | 5% of the tropospheric frequency shift after combination* |
| Ionosphere influence residual | 10% of the ionospheric frequency shift after combination* |
| Position accuracy of CSS | ± 0.1 m |
| Velocity accuracy of CSS | $\pm 1.0 \times 10^{-3}$ m/s |
| Gravitational potential model accuracy | $\pm 0.3 \text{ m}^2/\text{s}^2$ (CSS), $\pm 0.1 \text{ m}^2/\text{s}^2$ (ground) |
| Tide influence residual | $0.1 \text{ m}^2/\text{s}^2$ |

*: Combination of up and down frequency signals, expressed as eq.(2)

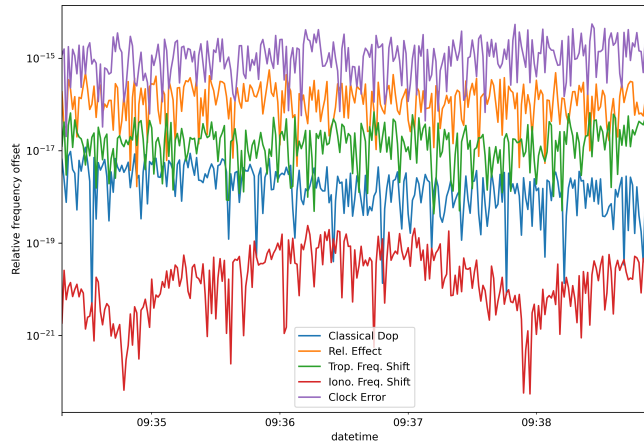


FIG. 4. Relative frequency offset between theoretical predictions and simulated observations of frequency shift during one slot period (around 5 min, from June 01, 09:34:18 to June 01, 09:38:52). The main error influence factors are denoted in different colors, marked in the left-bottom corner. The most prominent error source is the clock error, at least two magnitudes larger than other error influences.

itational potential difference between the CSS and the ground station. Based on this formulation, simulation results have shown that the GRS could be tested at around 2×10^{-7} , at least two orders in magnitude higher than the presently highest accuracy level. In addition, the proposed formulation in this study could be a new approach applied to determining the geopotential difference between arbitrary two ground stations. In contrast, the conventional approach is gravimetry plus leveling [32], which is laborious and low-efficient [33]. Suppose two ground stations equipped with optical clocks with the stability of 1×10^{-18} can simultaneously observe the frequency signals from CSS, the accuracy of determining the geopotential difference between the two ground stations could achieve a level of $0.1 \text{ m}^2/\text{s}^2$, because sub-

traction of the observation between CSS and one station and that between CSS and another station will cancel the common error sources stemming from CSS. With the rapid development of time-frequency science, the optical-atomic clocks with unprecedented accuracy and stability

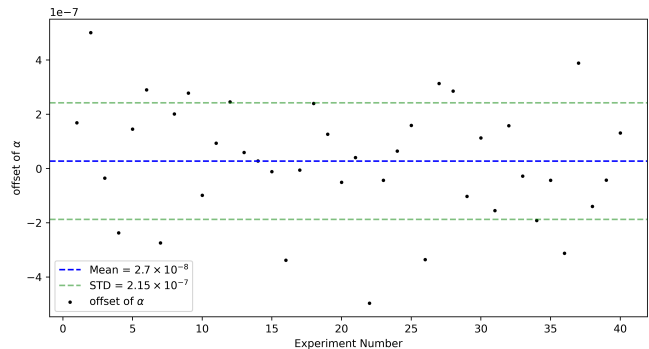


FIG. 5. The results of 40 different simulation experiments. In each experiment, we use the same parameters as listed in Table I with different random seeds of errors generation.

have been generated [34–39]. It dramatically expands the clocks’ application scopes in various branches. Besides its application in geopotential determination, this formulation can also be applied in height propagation between two datum stations separated by oceans, unifying the vertical height systems around the world [33].

ACKNOWLEDGMENTS

This study is supported by the National Natural Science Foundation of China (NSFC) (Grant Nos. 42030105, 41721003, 41631072, 41874023, 41804012, 41974034), Space Station Project (Grant No. 2020-228), and Natural Science Foundation of Hubei Province (Grant No. 2019CFB611).

[1] R. F. C. Vessot and M. W. Levine, General relativity and gravitation **10**, 181 (1979).

[2] M. Takamoto, I. Ushijima, N. Ohmae, T. Yahagi, K. Kokado, H. Shinkai, and H. Katori, Nature Photonics

- 14, 411 (2020).
- [3] R. F. C. Vessot, M. W. Levine, E. M. Mattison, E. L. Blomberg, T. E. Hoffman, G. U. Nystrom, B. F. Farrell, R. Decher, P. B. Eby, C. R. Baugher, J. W. Watts, D. L. Teuber, and F. D. Wills, *Physical Review Letters* **45**, 2081 (1980).
- [4] J. Kouba, *GPS Solutions* **25**, 1 (2021).
- [5] P. Delva, N. Puchades, E. Schönemann, F. Dilssner, C. Courde, S. Bertone, F. Gonzalez, A. Hees, C. Le Poncin-Lafitte, F. Meynadier, R. Prieto-Cerdeira, B. Sohet, J. Ventura-Traveset, and P. Wolf, *Phys. Rev. Lett.* **121**, 231101 (2018).
- [6] S. Herrmann, F. Finke, M. Lülf, O. Kichakova, D. Puetzfeld, D. Knickmann, M. List, B. Rievers, G. Giorgi, C. Günther, H. Dittus, R. Prieto-Cerdeira, F. Dilssner, F. Gonzalez, E. Schonemann, J. Ventura-Traveset, and C. Lammerzähl, *Physical review letters* **121**, 231102 (2018).
- [7] L. Cacciapuoti and C. Salomon, in *Journal of Physics: Conference Series*, Vol. 327 (IOP Publishing, 2011) p. 012049.
- [8] F. Meynadier, P. Delva, C. le Poncin-Lafitte, C. Guerlin, and P. Wolf, *Classical and Quantum Gravity* **35**, 035018 (2018).
- [9] L. Blanchet, C. Salomon, P. Teyssandier, and P. Wolf, *Astronomy & Astrophysics* **370**, 320 (2001).
- [10] B. Linet and P. Teyssandier, *Phys. Rev. D* **66**, 024045 (2002).
- [11] X. Sun, W.-B. Shen, Z. Shen, C. Cai, W. Xu, and P. Zhang, *The European Physical Journal C* **81**, 1 (2021).
- [12] Z. Shen, W.-B. Shen, T. Zhang, L. He, Z. Cai, X. Tian, and P. Zhang, *Advances in Space Research* **68**, 2776 (2021).
- [13] Y. M. Guo, in *The 12th China Satellite Navigation Conference, CSNC 2021* (2021).
- [14] W. B. Wang, in *The 12th China Satellite Navigation Conference, CSNC 2021* (2021).
- [15] R. S. Elliot, *IEEE Transactions on Antennas and Propagation* **31**, 1 (1983).
- [16] M. M. Hoque and N. Jakowski, *Global navigation satellite systems: signal, theory and applications* **10**, 30090 (2012).
- [17] K. Schüller, *Program System ETERNA-x et34-x-v80* for Earth and Ocean Tides Analysis and Prediction* (2020).
- [18] T. Hartmann and H.-G. Wenzel, *Geophysical research letters* **22**, 3553 (1995).
- [19] H.-G. Wenzel, *Tidal phenomena*, 9 (1997).
- [20] B. Hoffmann, *Physical Review* **121**, 337 (1961).
- [21] D. Kleppner, R. F. C. Vessot, and N. F. Ramsey, *Astrophysics and Space Science* **6**, 13 (1970).
- [22] J. Saastamoinen, *The use of artificial satellites for geodesy* **15**, 247 (1972).
- [23] J. Böhm and H. Schuh, *Vienna mapping functions* (na, 2003).
- [24] D. Bilitza, K. Rawer, L. Bossy, and T. Gulyaeva, *Advances in Space Research* **13**, 15 (1993).
- [25] J. Baerenzung, M. Holschneider, J. Wicht, V. Lesur, and S. Sanchez, *Earth, Planets and Space* **72**, 1 (2020).
- [26] G. Petit and B. Luzum, *IERS conventions (2010)*, Report (Bureau International des Poids et mesures sevres (france), 2010).
- [27] N. K. Pavlis, S. A. Holmes, S. C. Kenyon, and J. K. Factor, in *AGU Fall Meeting Abstracts* (2008).
- [28] L. Weiping, Q. Hongxing, and D. Qi, in *2012 IEEE International Conference on Information and Automation (IEEE, 2012)* pp. 811–813.
- [29] N. K. Pavlis, S. A. Holmes, S. C. Kenyon, and J. K. Factor, *Journal of geophysical research: solid earth* **117**, 1 (2012).
- [30] D. W. Allan, M. A. Weiss, and J. L. Jespersen, in *Proceedings of the 45th Annual Symposium on Frequency Control 1991* (IEEE, 1991) pp. 667–678.
- [31] D. Bilitza, D. Altadill, V. Truhlik, V. Shubin, I. Galkin, B. Reinisch, and X. Huang, *Space weather* **15**, 418 (2017).
- [32] W. A. Heiskanen and H. Moritz, *Physical geodesy(Book on physical geodesy covering potential theory, gravity fields, gravimetric and astrogeodetic methods, statistical analysis, etc)* (W. H. Freeman and Company San Francisco, 1967).
- [33] Z. Shen, W.-B. Shen, and S. Zhang, arXiv preprint arXiv:2008.05868, 1 (2020).
- [34] T. L. Nicholson, S. L. Campbell, R. B. Hutson, G. E. Marti, B. J. Bloom, R. L. McNally, W. Zhang, M. D. Barrett, M. S. Safronova, G. F. Strouse, *et al.*, *Nature communications* **6**, 1 (2015).
- [35] N. Huntemann, C. Sanner, B. Lipphardt, C. Tamm, and E. Peik, *Physical review letters* **116**, 063001 (2016).
- [36] W. F. McGrew, X. Zhang, R. J. Fasano, S. A. Schäffer, K. Beloy, D. Nicolodi, R. C. Brown, N. Hinkley, G. Milani, M. Schioppo, T. H. Yoon, and A. D. Ludlow, *Nature* **564**, 87 (2018).
- [37] E. Oelker, R. B. Hutson, C. J. Kennedy, L. Sonderhouse, T. Bothwell, A. Goban, D. Kedar, C. Sanner, J. M. Robinson, G. E. Marti, *et al.*, *Nature Photonics* **13**, 714 (2019).
- [38] T. Nakamura, J. Davila-Rodriguez, H. Leopardi, J. A. Sherman, T. M. Fortier, X. Xie, J. C. Campbell, W. F. McGrew, X. Zhang, Y. S. Hassan, *et al.*, *Science* **368**, 889 (2020).
- [39] S. M. Brewer, J.-S. Chen, A. M. Hankin, E. R. Clements, C.-W. Chou, D. J. Wineland, D. B. Hume, and D. R. Leibrandt, *Physical review letters* **123**, 033201 (2019).